Title

Physical properties of the cytoplasm modulate the rates of microtubule growth and shrinkage

Authors

Molines A. T.[1,7] *, Lemière J.[1], Edrington C.H.[2], Hsu C-T. [3], Steinmark I.E. [4], Suhling K. [4], Goshima G.[5,7], Holt L.[6,7], Brouhard G. J.[2,3], Chang F[1,7] *.

1. Department of Cell and Tissue Biology, University of California, San Francisco, United States.
2. Department of Biology, McGill University, Montréal, Quebec, Canada
3.Department of Physics, McGill University, Montréal, Quebec, Canada
4. Department of Physics, King's College London, UK
5. Sugashima Marine Biological Laboratory and Division of Biological Science, Graduate School of Science, Nagoya University, Japan
6. Institute for Systems Genetics, New York University Langone Health, New York, NY 10016, USA
7. Marine Biological Laboratory, Woods Hole, MA 02543

* Correspondence to: a.t.molines@gmail.com and fred.chang@ucsf.edu

Keywords

Cytoskeleton dynamics, microtubules, cytoplasm, crowding, viscosity, diffusion, fission yeast Schizosaccharomyces pombe

Abstract

The cytoplasm represents a crowded environment whose properties may change according to physiological or developmental states. Although the effects of crowding and viscosity on *in vitro* reactions have been well studied, if and how the biophysical properties of the cytoplasm impact cellular functions *in vivo* remain poorly understood. Here, we probed the effects of cytoplasmic concentration on microtubule (MT) dynamics by studying the effects of osmotic shifts in the fission yeast *Schizosaccharomyces pombe*. Increasing cytoplasmic concentration by hyperosmotic shock led to proportionate reductions in the rates of interphase MT growth and shrinkage. Conversely, dilution of the cytoplasm in hypoosmotic shifts led to proportionately faster rates. Numerous lines of evidence indicate that these effects were due to biophysical properties of the cytoplasm. These effects were recapitulated in *in vitro* reconstituted MT assays by modulating viscosity, not by crowding. Our findings suggest that even at normal conditions, the viscous properties of cytoplasm modulate the dynamic reactions of MT polymerization and depolymerization.

Introduction

The properties of the cytoplasm and its effects on cellular processes remain poorly understood. Cytoplasm is composed of 100-300 mg/ml of macromolecules (proteins, nucleic acids, lipids, etc), which occupy 10-40% of the total cellular volume (Milo & Phillips, Cell Biology by the Numbers, 2018). These components range in size from small globular proteins to extended networks of organelles and cytoskeletal polymers. Ribosomes alone occupy ~20% of that volume (Delarue et al., 2018). Biophysical studies reveal that these constituents form a porous-elastic material that allows diffusion of small molecules but impedes movement of larger particles (Luby-Phelps et al., 1986; Moeendarbary et al., 2013; Xiang et al., 2020), and molecular simulations suggest a highly dense packing of macromolecules (Yu et al., 2016) (Mcguffee and Elcock, 2010).

Unlike the density of inert matter, recent findings show that cytoplasmic density is not constant. Rather, cells regulate and vary their density as part of normal cell physiology: during the cell cycle, among different cell types, aging, nutritional responses and disease states (Neurohr and Amon, 2020). There is evidence though that the density of cytoplasm may be near functional limits (Dill et al., 2011) as increasing its concentration can lead to large effects including solidification of the cytoplasm (Heimlicher et al., 2019; Joyner et al., 2016; Munder et al., 2016). These density changes, which potentially affect cytoplasmic concentration and crowding effects, further underscore the importance of understanding effects of cytoplasmic concentration. How molecular reactions are able to function effectively within this crowded intracellular environment remains a critical open question.

There are several conceptual models used to describe the influence of macromolecular crowding. Minton and colleagues have argued that bulky crowding agents “exclude volume”, which increases the effective concentration and activity of other enzymes (Minton, 2006; Shahid et al., 2017). Nonspecific interactions between macromolecules in the cytoplasm can affect the rates and equilibria on reactions in numerous ways including macromolecular crowding, confinement and adsorption (Minton, 2006). Macromolecular crowding can impede movement, produce forces that draw molecules together, for instance to promote phase separation, as well as produce osmotic pressure within cells (Mitchison, 2019; R.John, 2001; Shahid et al., 2017). Although effects of crowding have been studied largely in theory and in *in vitro* experiments, the extent to which these theories and experiments apply to cellular reactions *in vivo* remains debatable. For example, Mitchison used the concept of colloidal osmotic pressure to argue that cytoplasm is functionally dilute, such that reactions such as microtubule (MT) polymerization are unaffected by crowding effects like excluded volume, perhaps because many macromolecules are well organized in large complexes (Mitchison, 2019). To distinguish between these concepts, what is needed are experiments that perturb the properties of cytoplasm and measure the rates of cellular reactions.

MT dynamic instability represents an attractive case with which to probe the effects of the cytoplasm on a defined molecular reaction *in vivo*. First, the polymerization and depolymerization of single MTs are reactions that can be quantitatively measured in living cells as microtubule length changes using microscopy. Second, the effects of macromolecular crowding on MTs *in vitro* are known, as are the effects of viscosity alone: MTs grow significantly faster in the presence of bulky crowders like polyethylene glycol but significantly slower in the presence of small viscous agents like glycerol (Wieczorek et al., 2013). These *in vitro* measurements can be compared to *in vivo* measurements when considering mechanisms. Third, the mechanisms driving MT dynamics have been extensively studied, and the biological importance of these dynamics is well established. At 100 kDa in mass and 8 nm in length, the tubulin dimer represents a size

range typical for soluble proteins and enzymes. Finally, MT polymerization is dependent on tubulin concentration while MT depolymerization is not (Fygenson et al., 1994; Walker et al., 1988). Thus, changes in tubulin concentration (e.g., because of changes in cytoplasmic concentration) should impact polymerization alone, which is a testable prediction of some models. Taken together, microtubule dynamic instability is well-suited to discover which properties of cytoplasm are having the strongest impact on cellular reactions, and more generally, to inform biophysical models describing the physical properties of cytoplasm. As the cytoplasm may exhibit both crowding and viscous properties, studying which of these (or other properties) affect reactions such as MT growth and shrinkage *in vivo* may elucidate relevant properties of the cytoplasm.

Fission yeast is an excellent model organism with which to study the physical regulation of MT dynamics *in vivo*. We can readily image the interphase microtubule bundles and measure the dynamic behavior of individual microtubules with precision (Höög et al., 2007; Loiodice et al., 2019; Sawin and Tran, 2006). Importantly, we can readily manipulate the properties of their cytoplasm using osmotic shifts, which create robust and well characterized changes in cellular volume and cytoplasm concentration (Atilgan et al., 2015; Knapp et al., 2019).

Here, we study the effects of the properties of the cytoplasm on MTs in fission yeast by using osmotic shifts to vary cytoplasmic concentration. We show that hyperosmotic shifts, which increase cytoplasmic concentration, lead to dampening and "freezing" of MT growth and shrinkage. Conversely, hypoosmotic shifts, which decrease cytoplasmic concentration, lead to increased rates of MT polymerization and depolymerization. The observed MT effects, which were independent of the osmotic stress response and key microtubule regulators, correlated with global changes in cytoplasmic biophysical properties and were recapitulated *in vitro* through modulation of viscosity and *in silico* by variation the association rate constant. These findings demonstrate that cytoplasm is not functionally dilute but modulates MT dynamics through viscous effects even at normal concentrations of cytoplasm.

Results

Cytoplasm concentration tunes microtubule dynamics

The density of cellular components in a cell can be experimentally manipulated by varying its osmotic environment (Knapp et al., 2019). We treated live fission yeast cells with an external osmotic agent (addition of sorbitol in the growth medium), which led to an acute loss of cell volume in a dose-dependent, reversible manner (Fig. 1 A and B) (Sup. Fig. 1 and Sup. Fig. 2) (Atilgan et al., 2015; Knapp et al., 2019). For instance, 1 M sorbitol in YE (YE5S rich medium) caused cells to decrease 40% in volume, while 1.5 M sorbitol led to a 60% decrease in volume, all without loss in cell viability (Sup. Fig. 1). This volume loss presumably occurs through water loss. Increases in fluorescence intensity of GFP-labeled tubulin and a ribosomal protein confirmed that cytoplasmic proteins increased in concentration inversely proportional to volume changes (Sup. Fig. 1).

Having validated this approach to alter cytoplasmic concentration, we applied it to cells expressing GFP-tubulin. Hyperosmotic shifts caused striking effects on the dynamic behaviors of interphase MTs, as noted previously (Robertson and Hagan, 2008; Tatebe et al., 2005). We found that in acute response to sorbitol shifts, the interphase MT cytoskeleton was largely maintained (Fig. 1 A). Time lapse imaging showed that while interphase MTs in untreated cells were characteristically dynamic with little time in pause, increasing concentrations of sorbitol caused MTs to "freeze", especially at high sorbitol

concentrations (1.5 M) (Fig. 1 B, C and D). In general, MTs were paused at various lengths and exhibited little or no growth or shrinkage. To determine whether the observed sorbitol effects were reversible, we treated cells with osmotic oscillations in which sorbitol-containing medium was introduced and then replaced with medium lacking sorbitol in repeated cycles at 5-min intervals. Upon each hyperosmotic shift to 1.5 M sorbitol, most of the MTs were "frozen" within 30 sec (Fig. 1 B and C). Upon shift back to sorbitol-free medium, within 30 s, all interphase MTs started to shrink toward the middle of the cell, and then regrew back in <10 min (Fig. 1 B and Sup. Fig. 2), consistent with previous observations (Alasdair and Hagan, 2008). This uniform shrinkage may be a consequence of the loss of the stabilizing MT GTP cap during the frozen state. This cycle of MT "freezing" and resumption of dynamics occurred repeatedly (Sup. Fig. 2), demonstrating that the effects of sorbitol were rapid (timescales <30 s) and reversible.

The effects on MT dynamics were dependent on the sorbitol concentration. We detected progressive increases in both the time that MTs spent in a pause state (Fig. 1 C) and the number of MTs in a pause state (Sup. Fig. 3). At 1 M sorbitol, ~20% of MTs were frozen, while at 1.5 M, 70% of MTs appeared frozen over the observation period (Sup. Fig. 3). Of the MTs that continued to be dynamic, their rates of polymerization and depolymerization decreased in a sorbitol dose-dependent manner (Fig. 1 C, E, and F, and Sup. Fig. 3). Importantly, sorbitol's effects on MT polymerization and depolymerization were proportional; for instance, at 1 M sorbitol, both polymerization and depolymerization rates decreased by ~40% (Fig. 1 E and F). Treatment with high sorbitol also made MTs resistant to depolymerization by cold temperature (Sup. Fig. 4), further indicating that these MTs were in a highly stabilized state.

We next asked whether hypoosmotic shifts, which effectively dilute the cytoplasm, yield effects on MT dynamics opposite to those prompted by hyperosmotic shifts. Our initial attempts to swell intact fission yeast cells with hypoosmotic shifts were not successful: cells did not increase in volume very much and any effects were transient, possibly because the cell wall impeded swelling (Nakayama et al., 2012). However, protoplasts (cells with the cell wall removed) swelled substantially in response to hypoosmotic shifts without lysing (Fig. 2 A) (Lemière and Berro, 2018). Shifting protoplasts to hypotonic and hypertonic conditions led to predictable changes in cell volume over a ~2.5-fold range (Fig. 2 A). We determined that protoplasts prepared in 0.4 M sorbitol in YE medium were in isotonic conditions, as their average volume matched that of intact cells in YE medium without sorbitol, and the diffusion rates of GEMs (or nano) particles also matched those in intact cells (see below and Methods). MTs were detectable in protoplasts across all volumes (Fig. 2 B). Hyperosmotic shifts in protoplasts led to proportionate decrease in MT polymerization and depolymerization rates, similar to what was observed in cells with an intact cell wall (Fig. 2 C to F). In hypoosmotic shifts, MT polymerization and depolymerization rates increased proportionally over isotonic conditions (Fig. 2 C to F). Notably, when cell volume increased by ~40 % over isotonic conditions (corresponding to a ~30% dilution of the cytoplasm), both MT polymerization and depolymerization rates increased by ~50% (Fig. 2 E and F). This result implies that cytoplasm dampens the rates of MT polymerization and depolymerization at "normal" cytoplasmic concentration.

To evaluate whether these effects arise in other cell types, we performed similar osmotic shifts with the moss *Physcomitrium (Physcomitrella) patens*. Caulonema cells expressing mCherry-labelled tubulin and citrine-labelled EB1 displayed lower MT polymerization and depolymerization rates when the osmolarity of the medium was increased with sorbitol (Sup. Fig. 5). This conservation suggested that these effects arise from conserved properties of the cytoplasm.

Normalization of the MT polymerization and depolymerization rates to the isotonic conditions for both yeast cells and protoplasts revealed how changes in the concentration of the cytoplasm, above and below normal levels, caused similar graded responses for MT polymerization and depolymerization (Fig. 2 E and F). This proportionate response suggests that the property of the cytoplasm that is changed by osmotic shocks affects both MT polymerization and depolymerization in a similar manner. Interestingly, MT dynamics decreased when the cytoplasm concentration and tubulin concentration increased (Fig. 1 and 2), opposite to what would be expected if crowding or tubulin concentration were responsible for MT dynamics.

Effect of osmotic shifts on MT dynamics is independent of stress response and regulatory proteins at MT plus ends

We next investigated several plausible mechanisms for these effects of the cytoplasm on MT dynamics. We first considered indirect mechanisms that operate through osmotic shock response pathways (such as regulation through phosphorylation) and/or regulation by MT regulators at the MT plus end.

First, we tested whether MT stabilization is a downstream effect of an osmotic stress response pathway. Cells exhibit osmotic stress responses that allow them to adapt and survive stresses; the MAP kinase Sty1 (Hog1, p38 ortholog) is a master integrator of multiple stress pathways (Perez and Cansado, 2011). Sorbitol-mediated osmotic shifts applied to *sty1*Δ cells caused a decrease in MT dynamics (Sup. Fig. 6) very similar to the decrease observed in wild-type cells (Fig. 1) as previously observed (Robertson and Hagan, 2008). Other triggers of the Sty1 stress pathways, such as latrunculin A, do not produce MT "freezing" (Daga et al., 2006). Thus, "freezing" of the MT network is not a downstream response of Sty1-dependent stress pathways.

We next explored the role of MT regulatory proteins at MT plus ends (+TIPs). These proteins could cap and stabilize MTs during hyperosmotic shifts and/or drive more rapid dynamics during hypo-osmotic shifts. Numerous +TIP proteins have been characterized in fission yeast, with the major classes represented by the EB-family +TIP protein Mal3 (EB1) that binds the GTP-cap and the XMAP215-family polymerase Alp14 (XMAP215) (Akhmanova and Steinmetz, 2010; Al-Bassam et al., 2012; Busch and Brunner, 2004) . In hyperosmotic shifts, *mal3*Δ and *alp14*Δ mutant cells exhibited similar dampening of MT dynamics as wild-type cells (Sup. Fig. 7). As most other +TIP proteins are dependent on Mal3 for localization these two mutants effectively capture the function of most of the +TIPs; therefore, the stabilization is not dependent on these +TIPs. Imaging during hyperosmotic shifts showed that Alp14-GFP was maintained at the MT plus ends during the shift, but Mal3-GFP localization to plus ends decreased (Sup. Fig. 8), consistent with hydrolysis of the GTP-cap (Guesdon et al., 2016) which explains the rapid collapse of the MT following reversal of the osmotic shock (Fig. 1 B and Sup. Fig. 2).

Taken together, these observations demonstrate that the acute effect of increased cytoplasm concentration on MT dynamics observed here is independent of the osmotic stress response and the presence of +TIPs. An attractive alternative model is that the assembly and disassembly of MTs are affected directly by biophysical properties of the cytoplasm that scale with its concentration.

Cytoplasm concentration modulates nanoparticles diffusion

To characterize how osmotic shifts affect the biophysical properties of the cytoplasm, we carried out microrheology experiments with GEMs. GEMs are spherical nanoparticles of defined sizes composed

of fluorescently labeled non-eukaryotic proteins (Delarue et al., 2018). We expressed gene fusions encoding GEMs fused with the Sapphire fluorescent protein in fission yeast (Methods) and imaged them at rapid frame rates (~100 fps) to analyze their motion (Fig. 3 A). We analyzed GEMs of a range of sizes (20, 40, and 50 nm in diameter) similar in scale to the widths of a MT (24 nm), a ribosome (~25 nm), a proteasome (~15 nm), and a XMAP215/Alp14-tubulin complex (19 nm diameter), but larger than a tubulin dimer (4 by 8 nm). Mean squared displacement (MSD) plots revealed that the movements of the GEMs were sub-diffusive ($\alpha < 1$) (Sup. Fig. 9), as observed in other cell types (Delarue et al., 2018). The effective diffusion coefficients (D_{eff}) extracted from the MSD plots showed that GEMs motion was size-dependent: larger particles diffused more slowly than the smaller GEMs (Fig. 3 B), consistent with previous rheological observations in other cell types (Luby-Phelps et al., 1986) (Moeendarbary et al., 2013).

Having characterized GEMs motion in yeast cells, we measured the impact of osmotic shocks on their diffusion. At 1 M sorbitol, 40-nm GEMs and 50-nm GEMs were effectively immobile, while 20-nm GEMs still moved (Fig. 3 B). At 1.5 M sorbitol, GEMs of all three sizes largely stopped moving in the cytoplasm (Fig. 3 B).

We also analyzed the motion of the 40-nm GEM in protoplasts to investigate the effect of hypoosmotic shocks, which decrease cytoplasm concentration on GEMs diffusion. We confirmed that the D_{eff} values for GEMs in protoplasts exposed to 0.4 M sorbitol were similar to those in intact cells (Fig. 3 D), consistent with this concentration being the isotonic point of the normal cytoplasm. GEMs mobility increased in hypoosmotic shifts (Fig. 3 C), consistent with decreased cytoplasm concentration and decreased in hyperosmotic shifts, consistent with increased cytoplasm concentration. These observations on yeast cells and protoplasts suggest that osmotic shifts caused substantial changes in cytoplasm biophysical properties.

Normalization of GEMs diffusion to the isotonic condition in yeast and protoplasts revealed that osmotic shifts affect MT dynamics and the diffusion of nanoparticles within the cytoplasm in roughly similar manners (Fig. 3 D), further supporting the hypothesis that physical properties of the cytoplasm affect both GEMs and MTs. Both followed the general inverse trend of slower dynamics with increasing cytoplasmic concentration. Thus, the GEMs data show that general biophysical properties of the cytoplasm (encountered by particles the size of GEMs) correspond with the changes in MT dynamics. during osmotic shifts. The slower diffusion of GEMs throughout the cytoplasm in hyperosmotic shifts suggests that diffusion of even smaller proteins like tubulin may also be slower in these conditions.

Microtubule dynamics scale with tubulin diffusion in cells

As MT dynamics depend on the motion of tubulin subunits, we next directly assessed the effects of osmotic shifts on the diffusion of tubulin dimers. We measured the diffusion of soluble tubulin by fluorescence loss in photobleaching (FLIP) experiments. Fluorescence intensity in the cell is measured while a small region of the cell is repeatedly photobleached. The rate at which fluorescence decays over time is proportional to the diffusion of the fluorescent probe used (Ishikawa-Ankerhold et al., 2012). To our knowledge, the rate of tubulin diffusion has been measured only in sea urchin (Salmon et al., 1984) and in PTK2 cells (Wang et al., 2004). As a marker for soluble α/β tubulin dimers, we used Atb2-GFP (α-tubulin 2) expressed from the native chromosomal locus (Sato et al., 2009). Cells were treated with the MT inhibitor methyl benzimidazol-2-yl-carbamate to depolymerize MTs, and then we repeatedly photobleached a ~1 μm region of the cytoplasm (Fig. 4 A and B). We then measured the decay in GFP fluorescence in the cell (Methods).

To estimate the tubulin diffusion rate, we designed a 1D stochastic model of diffusion in which the only free parameter is tubulin diffusion (Methods). Comparison of the model predictions with our experimental data (Fig. 4 B) yielded an estimated diffusion rate of GFP-tubulin of 7 $\mu m^2 s^{-1}$ in cells in YE without sorbitol; very close to the value of ~6 $\mu m^2 s^{-1}$ obtained previously in other cell types (Salmon et al., 1984) (Wang et al., 2004). According to our model, diffusion rates decreased to 4 $\mu m^2 s^{-1}$ in YE + 1 M sorbitol and 1.5 $\mu m^2 s^{-1}$ in YE + 1.5 M sorbitol (Fig. 4 C); the latter value represents a decrease of up to 5x in tubulin dimer diffusion. Interestingly, these changes in tubulin diffusion were linearly correlated with the rates of MT polymerization and depolymerization (Fig. 4 D). Taken together, these data suggest that tubulin diffusion may constitute a rate-limiting factor in these circumstances (Discussion).

Viscosity limits microtubule dynamics

In order to determine whether changes in viscosity could explain the changes in tubulin diffusion and MT growth and shrinkage rates resulting from osmotic shifts, we measured the viscosity of the fission yeast cytoplasm. We estimated viscosity of the fission yeast cytoplasm using time-resolved Fluorescence Anisotropy Imaging (tr-FAIM) (Puchkov, 2012). This method measures the movement of a fluorescent dye (fluorescein) in the cytoplasm of living cells, assessing molecular movements of the size scale of the dye and water (see Methods; Sup. Fig. 10). Fitting and extraction of the rate constants and comparison to the calibration curve yielded a viscosity value of ~ 9 cP, which is in line with the broad range of previous viscosity measurements for eukaryotic cytoplasm (range from 1 to 50 cP) (Obodovskiy, 2019). This value suggests that the fission yeast cytoplasm has a viscosity similar to that of 53% (v/v) glycerol (in water). For cells treated with 1.5M sorbitol, we obtained a slightly higher value of 12 cP, corresponding to 57% (v/v) glycerol. This result suggests that the viscosity of the cytoplasm increases with its concentration following hyperosmotic shocks. As diffusion scales inversely with viscosity, such changes in viscosity may explain the effects of the osmotic shift on GEMs and tubulin diffusion rates.

In order to isolate the effects of viscosity alone on MT dynamics, we repeated these experiments in a reconstituted system. (Fig. 5 A). Although it was previously shown that viscosity decreases MT polymerization rates *in vitro* (Wieczorek et al., 2013) the constrains of the fluorescence-based MT dynamic assays used limited the time-lapse recording length and frequency and did not allow its effect on MT shrinkage rate to be quantitatively studied. We therefore took advantage of Interference Reflection Microscopy (IRM) to image MTs at 2 fps, allowing a more accurate quantification of shrinkage rates. We reconstituted MT dynamics in the presence of glycerol as a viscous agent using a well-established assay using purified tubulin (Fig. 5 A) (Gell et al., 2011). A range of glycerol concentrations was added to the reconstitutions (Wieczorek et al., 2013) to produce a range of viscosities from 0.7 to 1.5 cP. MT polymerization and depolymerization rates both decreased proportionally in a dose dependent manner with increasing viscosity (Fig. 5 B and C). Using viscosity of the buffer and the Stokes-Einstein equation we estimated tubulin diffusion in the reconstituted assay (see methods) and saw a linear relationship between both rates and tubulin diffusion (Fig 5. D). Thus, the proportional influence of cytoplasmic properties on MT growth and shrinkage rates that we observed *in vivo* may be reproduced *in vitro* by modulating a single parameter, viscosity.

To gain insight into how viscosity influences MT growth and shrinkage rates, we used a simple, 6 parameters model for MT dynamic instability (Hsu et al., 2020) that reproduces the core behaviors of polymerization, catastrophe, and depolymerization (Odde, 1997). In order to model the effect of viscosity, we varied the tubulin association rate constant k^+ (Fig 5. E), which defines the rate at which tubulin binds

to protofilament ends. All other parameters, notably bond energies of tubulin-tubulin bonds, remained constant. The model predicts that growth rates decrease with k^+, as expected from fewer binding events (Fig. 5 F). However, the model also predicts that depolymerization rates scale linearly with k^+ (Fig. 5 G), because when associate rate constants change, dissociation rate constants must also change if the bond energies (ΔG_{long} and ΔG_{lat}) are to remain constant. In other words, the model predicts that both rates scale with the association rate constant.

Thus, our *in vitro* and *in silico* experiments paint a consistent picture: that both MT growth and MT shrinkage scale linearly with viscosity. Remarkably, our purified components recapitulate the observations from fission yeast, protoplasts, and moss cells. In all models, rates of MT polymerization and depolymerization are linearly correlated, indicating a conserved ratio of growth to shrinkage (Fig. 5 H). The ratio is different in each case, presumably due to the specific conditions of each case (presence of MAPs, tubulin isoform properties, tubulin concentration, temperature, etc.). Nonetheless, the ratio is maintained when MT dynamics are perturbed, either by changes in cytoplasm concentration *in vivo*, changes in viscosity *in vitro*, or changes in the association rate constant *in silico*.

In addition, normalizing the rates from each model to the value in the unperturbed condition collapsed all the data onto a line which matches the *in silico* model prediction (Fig. 5 I). By varying a single parameter, k^+, the model is able to recapitulate the observations both qualitatively and quantitatively. This suggests that increasing viscosity of the environment is equivalent to reducing the association rate constant.

Discussion

Here we probed the effect of cytoplasm on MT dynamics *in vivo* using osmotic shifts. During hyperosmotic shifts that increase cytoplasm concentration, MTs paused more frequently and polymerized and depolymerized more slowly; at high concentrations, MTs appeared to largely "freeze" (Figure 1). Conversely, in hypoosmotic shock, which decrease cytoplasm concentration, MT polymerization and depolymerization rates speed up (Figure 2). We provide numerous lines of evidence to indicate that these effects act via the physical properties of the cytoplasm such as viscosity, as opposed to regulation of osmotic stress pathways or MT plus end regulators. The effects were acute (Fig. 1), reversible (Sup. Fig. 2) and scaled linearly with cytoplasm concentration in hypo- and hyperosmotic shocks (Fig. 3), strongly indicative of a physical response. The effects on MTs scaled with effects on the diffusive-like movement of GEMs and tubulin dimers. While MT "freezing" in response to hyperosmotic shocks has been noted previously in fission yeast (Tatebe et al., 2005)(Robertson and Hagan, 2008), we obtained two particularly significant results; MT dynamics scale linearly with cytoplasm concentration and, hypoosmotic shifts speed up MT polymerization and depolymerization rates. A significant implication is that even the "normal" concentration of cytoplasm dampens MT dynamic behaviors.

How might the cytoplasm influence MT dynamic behaviors? That MT polymerization and depolymerization are proportionally affected seems like an important clue. This coordinated effect on polymerization and depolymerization is unusual, as known perturbations such as changing tubulin concentration typically affect MT polymerization but not depolymerization rates (Fygenson et al., 1994). Although temperature (a purely physical concept) affects polymerization and depolymerization similarly (Fygenson et al., 1994). Modifying cytoplasmic concentration could alter many parameters including the concentration of molecules such as tubulin, their effective diffusion, viscosity and crowding effects. Our results are the opposite of the expected effects of altered tubulin concentration, which changes MT

polymerization rate without changing depolymerization rate (Fygenson et al., 1994). Similarly, our results are not consistent with crowding playing a decisive role, as addition of bulky crowding agents increase polymerization rate, not slow it down (Wieczorek et al., 2013) and prevent depolymerization (Bachand et al., 2018). This is consistent with a proposal in which macromolecular crowding effects may not be as dominant in the cytoplasm as previously perceived (Mitchison, 2019). Rather, our data support a hypothesis that the predominant effects of the cytoplasm on MT dynamics are via changes in viscosity and diffusion. Importantly, we show that changes in viscosity slow down MT polymerization and depolymerization linearly in a reconstituted system with purified components, similar to what we see *in vivo*,

Viscosity potentially affects multiple steps in MT polymerization and depolymerization. Viscosity inhibits diffusion of the tubulin dimer, which we show correlates with MT rates (Fig. 4 and 5). MT polymerization has been modeled as a two-step process depending on the rate of collision of tubulin dimer to the end of the protofilaments and the rate of incorporation into the tubule (Hsu et al., 2020; Wieczorek et al., 2013). Viscosity may also inhibit rate of conformational molecular changes, for instance in protofilament dynamics and in compaction of the tubulin dimer within the lattice (Brouhard and Rice, 2018).Our findings are in agreement with recent studies that suggest that similar conformational changes in the protofilaments occur in MT polymerization and depolymerization (Richard McIntosh et al., 2018) (Gudimchuk et al., 2020) (Brouhard and Rice, 2018).

In summary, we use MTs as an example to study how cytoplasmic properties affect biochemical reactions *in vivo* and discovered that viscosity plays a key role in regulating MTs dynamics. As the concentration and the density and other properties of the cytoplasm are known to vary during the cell cycle, in development, aging and diseases (Neurohr and Amon, 2020), it will be important to consider how cytoplasmic properties such as viscosity and crowding globally affect cytoskeletal and other cellular reactions.

References

Akhmanova A, Steinmetz MO. 2010. Microtubule +TIPs at a glance. *J Cell Sci*. doi:10.1242/jcs.062414

Al-Bassam J, Kim H, Flor-Parra I, Lal N, Velji H, Chang F. 2012. Fission yeast Alp14 is a dose-dependent plus end-tracking microtubule polymerase. *Mol Biol Cell* **23**:2878–2890. doi:10.1091/mbc.E12-03-0205

Ashford AJ, Hyman AA. 2006. Preparation of tubulin from porcine brainCell Biology, Four-Volume Set. Elsevier Inc. pp. 155–160. doi:10.1016/B978-012164730-8/50094-0

Atilgan E, Magidson V, Khodjakov A, Chang F, Author CB. 2015. Morphogenesis of the fission yeast cell through cell wall expansion Graphical abstract HHS Public Access Author manuscript. *Curr Biol* **25**:2150–2157. doi:10.1016/j.cub.2015.06.059

Bachand GD, Jain R, Ko R, Bouxsein NF, Vandelinder V. 2018. Inhibition of Microtubule Depolymerization by Osmolytes. *Biomacromolecules* **19**:2401–2408. doi:10.1021/acs.biomac.7b01799

Brouhard GJ, Rice LM. 2018. Microtubule dynamics: An interplay of biochemistry and mechanics. *Nat Rev Mol Cell Biol*. doi:10.1038/s41580-018-0009-y

Busch KE, Brunner D. 2004. The microtubule plus end-tracking proteins mal3p and tip1p cooperate for cell-end targeting of interphase microtubules. *Curr Biol* **14**:548–559. doi:10.1016/j.cub.2004.03.029

Daga RR, Yonetani A, Chang F. 2006. Asymmetric Microtubule Pushing Forces in Nuclear Centering. *Curr Biol* **16**:1544–1550. doi:10.1016/j.cub.2006.06.026

Delarue M, Brittingham GP, Pfeffer S, Surovtsev I V., Pinglay S, Kennedy KJ, Schaffer M, Gutierrez JI, Sang D, Poterewicz G, Chung JK, Plitzko JM, Groves JT, Jacobs-Wagner C, Engel BD, Holt LJ. 2018. mTORC1 Controls Phase Separation and the Biophysical Properties of the Cytoplasm by Tuning Crowding. *Cell* **174**:338-349.e20. doi:10.1016/j.cell.2018.05.042

Dill KA, Ghosh K, Schmit JD. 2011. Physical limits of cells and proteomes. doi:10.1073/pnas.1114477108

Flor-Parra I, Zhurinsky J, Bernal M, Gallardo P, Daga RR. 2014. A Lallzyme MMX-based rapid method for fission yeast protoplast preparation. *Yeast* **31**:61–66. doi:10.1002/yea.2994

Fygenson DK, Braun E, Libchaber A. 1994. Phase diagram of microtubules. *Phys*

Rev E. doi:10.1103/PhysRevE.50.1579

Gell C, Friel CT, Borgonovo B, Drechsel DN, Hyman AA, Howard J. 2011. Purification of tubulin from porcine brain. *Methods Mol Biol* **777**:15–28. doi:10.1007/978-1-61779-252-6_2

Gudimchuk NB, Ulyanov E V., O'Toole E, Page CL, Vinogradov DS, Morgan G, Li G, Moore JK, Szczesna E, Roll-Mecak A, Ataullakhanov FI, Richard McIntosh J. 2020. Mechanisms of microtubule dynamics and force generation examined with computational modeling and electron cryotomography. *Nat Commun* **11**. doi:10.1038/s41467-020-17553-2

Guesdon A, Bazile F, Buey RM, Mohan R, Monier S, García RR, Angevin M, Heichette C, Wieneke R, Tampé R, Duchesne L, Akhmanova A, Steinmetz MO, Chrétien D. 2016. EB1 interacts with outwardly curved and straight regions of the microtubule lattice. *Nat Cell Biol* **18**:1102–1108. doi:10.1038/ncb3412

Heimlicher MB, Bächler M, Liu M, Ibeneche-Nnewihe C, Florin EL, Hoenger A, Brunner D. 2019. Reversible solidification of fission yeast cytoplasm after prolonged nutrient starvation. *J Cell Sci* **132**. doi:10.1242/jcs.231688

Helenius J, Brouhard G, Kalaidzidis Y, Diez S, Howard J. 2006. The depolymerizing kinesin MCAK uses lattice diffusion to rapidly target microtubule ends. *Nature* **441**:115–119. doi:10.1038/nature04736

Höög JL, Schwartz C, Noon AT, O'Toole ET, Mastronarde DN, McIntosh JR, Antony C. 2007. Organization of Interphase Microtubules in Fission Yeast Analyzed by Electron Tomography. *Dev Cell* **12**:349–361. doi:10.1016/j.devcel.2007.01.020

Hsu CT (Jimmy), Brouhard GJ, François P. 2020. Numerical Parameter Space Compression and Its Application to Biophysical Models. *Biophys J* **118**:1455–1465. doi:10.1016/j.bpj.2020.01.023

Hyman AA. 1991. Preparation of marked microtubules for the assay of the polarity of microtubule-based motors by fluorescenceJournal of Cell Science. pp. 125–127. doi:10.1242/jcs.1991.supplement_14.25

Ishikawa-Ankerhold HC, Ankerhold R, Drummen GPC. 2012. Advanced fluorescence microscopy techniques-FRAP, FLIP, FLAP, FRET and FLIM. *Molecules*. doi:10.3390/molecules17044047

Joyner RP, Tang JH, Helenius J, Dultz E, Brune C, Holt LJ, Huet S, Müller DJ, Weis K. 2016. A glucose-starvation response regulates the diffusion of

macromolecules. *Elife* **5**. doi:10.7554/eLife.09376

Knapp BD, Odermatt P, Rojas ER, Cheng W, He X, Huang KC, Chang F. 2019. Decoupling of Rates of Protein Synthesis from Cell Expansion Leads to Supergrowth. *Cell Syst* **9**:434-445.e6. doi:10.1016/j.cels.2019.10.001

Kozgunova E, Goshima G. 2019. A versatile microfluidic device for highly inclined thin illumination microscopy in the moss Physcomitrella patens. *Sci Rep* **9**:1–8. doi:10.1038/s41598-019-51624-9

Kuimova MK, Yahioglu G, Levitt JA, Suhling K. 2008. Molecular rotor measures viscosity of live cells via fluorescence lifetime imaging. *J Am Chem Soc* **130**:6672–6673. doi:10.1021/ja800570d

Lemière J, Berroa J. 2018. Adaptation of actin dynamics and membrane tension control for yeast endocytosis. *bioRxiv* 342030. doi:10.1101/342030

Loiodice I, Janson ME, Tavormina P, Schaub S, Bhatt D, Cochran R, Czupryna J, Fu C, Tran PT. 2019. Quantifying tubulin concentration and microtubule number throughout the fission yeast cell cycle. *Biomolecules* **9**. doi:10.3390/biom9030086

Luby-Phelps K, Taylor DL, Lanni F. 1986. Probing the structure of cytoplasm. *J Cell Biol*. doi:10.1083/jcb.102.6.2015

Machado S, Mercier V, Chiaruttini N. 2019. LimeSeg: A coarse-grained lipid membrane simulation for 3D image segmentation. *BMC Bioinformatics* **20**:2. doi:10.1186/s12859-018-2471-0

Mahamdeh M, Howard J. 2019. Implementation of interference reflection microscopy for label-free, high-speed imaging of microtubules. *J Vis Exp* **2019**. doi:10.3791/59520

Maundrell K. 1990. nmt1 of fission yeast. A highly transcribed gene completely repressed by thiamine. *J Biol Chem* **265**:10857–10864.

Mcguffee SR, Elcock AH. 2010. Diffusion, Crowding & Protein Stability in a Dynamic Molecular Model of the Bacterial Cytoplasm. *PLoS Comput Biol* **6**:1000694. doi:10.1371/journal.pcbi.1000694

Minton AP. 2006. How can biochemical reactions within cells differ from those in test tubes? *J Cell Sci* **119**:2863–2869. doi:10.1242/jcs.03063

Mitchison TJ. 2019. Colloid osmotic parameterization and measurement of subcellular crowding. *Mol Biol Cell*. doi:10.1091/mbc.E18-09-0549

Moeendarbary E, Valon L, Fritzsche M, Harris AR, Moulding DA, Thrasher AJ, Stride E, Mahadevan L, Charras GT. 2013. The cytoplasm of living cells behaves as a poroelastic material. *Nat Mater*. doi:10.1038/nmat3517

Moreno S, Klar A, Nurse P. 1991. Molecular genetic analysis of fission yeast Schizosaccharomyces pombe. *Methods Enzymol* **194**:795–823. doi:10.1016/0076-6879(91)94059-L

Munder MC, Midtvedt D, Franzmann T, Nüske E, Otto O, Herbig M, Ulbricht E, Müller P, Taubenberger A, Maharana S, Malinovska L, Richter D, Guck J, Zaburdaev V, Alberti S. 2016. A pH-driven transition of the cytoplasm from a fluid- to a solid-like state promotes entry into dormancy. *Elife* **5**. doi:10.7554/eLife.09347

Nakayama Y, Yoshimura K, Iida H. 2012. Organellar mechanosensitive channels in fission yeast regulate the hypo-osmotic shock response. *Nat Commun* **3**:1007–1010. doi:10.1038/ncomms2014

Neurohr GE, Amon A. 2020. Relevance and Regulation of Cell Density. *Trends Cell Biol*. doi:10.1016/j.tcb.2019.12.006

Obodovskiy I. 2019. Basics of BiologyRadiation. Elsevier. pp. 429–445. doi:10.1016/b978-0-444-63979-0.00034-3

Odde DJ. 1997. Estimation of the Diffusion-Limited Rate of Microtubule Assembly, Biophysical Journal.

Perez P, Cansado J. 2011. Cell Integrity Signaling and Response to Stress in Fission Yeast. *Curr Protein Pept Sci* **11**:680–692. doi:10.2174/138920310794557718

Puchkov EO. 2012. Single yeast cell vacuolar milieu viscosity assessment by fluorescence polarization microscopy with computer image analysis. *Yeast* **29**:185–190. doi:10.1002/yea.2899

R.John E. 2001. Macromolecular crowding: obvious but underappreciated. *Trends Biochem Sci* **26**:597–604. doi:10.1016/s0968-0004(01)01938-7

Richard McIntosh J, O'Toole E, Morgan G, Austin J, Ulyanov E, Ataullakhanov F, Gudimchuk N. 2018. Microtubules grow by the addition of bent guanosine triphosphate tubulin to the tips of curved protofilaments. *J Cell Biol* **217**:2691–2708. doi:10.1083/jcb.201802138

Robertson AM, Hagan IM. 2008. Stress-regulated kinase pathways in the recovery tip growth and microtubule dynamics following osmotic stress in S. pombe. *J*

Cell Sci **121**:4055–4068. doi:10.1242/jcs.034488

Salmon ED, Saxton WM, Leslie RJ, Karow ML, McIntosh JR. 1984. Diffusion coefficient of fluorescein-labeled tubulin in the cytoplasm of embryonic cells of a sea urchin: Video image analysis of fluorescence redistribution after photobleaching. *J Cell Biol* **99**:2157–2164. doi:10.1083/jcb.99.6.2157

Sato M, Toya M, Toda T. 2009. Visualization of fluorescence-tagged proteins in fission yeast: The analysis of mitotic spindle dynamics using GFP-tubulin under the native promoter. *Methods Mol Biol* **545**:185–203. doi:10.1007/978-1-60327-993-2_11

Sawin KE, Tran PT. 2006. Cytoplasmic microtubule organization in fission yeast. *Yeast*. doi:10.1002/yea.1404

Schindelin J, Arganda-Carreras I, Frise E, Kaynig V, Longair M, Pietzsch T, Preibisch S, Rueden C, Saalfeld S, Schmid B, Tinevez JY, White DJ, Hartenstein V, Eliceiri K, Tomancak P, Cardona A. 2012. Fiji: An open-source platform for biological-image analysis. *Nat Methods*. doi:10.1038/nmeth.2019

Schneider CA, Rasband WS, Eliceiri KW. 2012. NIH Image to ImageJ: 25 years of image analysis. *Nat Methods*. doi:10.1038/nmeth.2089

Shahid S, Hassan MI, Islam A, Ahmad F. 2017. Size-dependent studies of macromolecular crowding on the thermodynamic stability, structure and functional activity of proteins: in vitro and in silico approaches. *Biochim Biophys Acta - Gen Subj* **1861**:178–197. doi:10.1016/j.bbagen.2016.11.014

Steinmark IE, Chung P, Ziolek RM, Cornell B, Smith P, Levitt JA, Tregidgo C, Molteni C, Yahioglu G, Lorenz CD, Suhling K. 2020. Time-Resolved Fluorescence Anisotropy of a Molecular Rotor Resolves Microscopic Viscosity Parameters in Complex Environments. *Small* **16**:1907139. doi:10.1002/smll.201907139

Suhling K, Levitt J, Chung PH. 2014. Time-resolved fluorescence anisotropy imaging. *Methods Mol Biol* **1076**:503–519. doi:10.1007/978-1-62703-649-8_22

Tatebe H, Shimada K, Uzawa S, Morigasaki S, Shiozaki K. 2005. Wsh3/Tea4 is a novel cell-end factor essential for bipolar distribution of tea1 and protects cell polarity under environmental stress in S. pombe. *Curr Biol* **15**:1006–1015. doi:10.1016/j.cub.2005.04.061

Walker RA, O'Brien ET, Pryer NK, Soboeiro MF, Voter WA, Erickson HP, Salmon ED. 1988. Dynamic instability of individual microtubules analyzed by

video light microscopy: rate constants and transition frequencies. *J Cell Biol* **107**:1437–1448. doi:10.1083/jcb.107.4.1437

Wang Z, Shah J V., Chen Z, Sun C-H, Berns MW. 2004. Fluorescence correlation spectroscopy investigation of a GFP mutant-enhanced cyan fluorescent protein and its tubulin fusion in living cells with two-photon excitation. *J Biomed Opt* **9**:395. doi:10.1117/1.1646416

Wieczorek M, Chaaban S, Brouhard GJ. 2013. Macromolecular crowding pushes catalyzed microtubule growth to near the theoretical limit. *Cell Mol Bioeng* **6**:383–392. doi:10.1007/s12195-013-0292-9

Xiang Y, Surovtsev I, Chang Y, Govers S, Parry B, Liu J, Jacobs-Wagner C. 2020. Solvent quality and chromosome folding in Escherichia coli. *bioRxiv* 2020.07.09.195560. doi:10.1101/2020.07.09.195560

Yamada M, Miki T, Goshima G. 2016. Imaging mitosis in the moss Physcomitrella patensMethods in Molecular Biology. Humana Press Inc. pp. 263–282. doi:10.1007/978-1-4939-3542-0_17

Yu I, Mori T, Ando T, Harada R, Jung J, Sugita Y, Feig M. 2016. Biomolecular interactions modulate macromolecular structure and dynamics in atomistic model of a bacterial cytoplasm. *Elife* **5**:1–22. doi:10.7554/eLife.19274

Material and methods

Fission yeast, media, and growth conditions

Standard methods for growing and genetically manipulating *Schizosaccharomyces pombe* were used (Moreno et al., 1991). For most experiments, cells were grown overnight in Yeast Extract (YE5S) medium to exponential phase (0.2<OD<0.8 at 600nm) with shaking at 30 °C. See Sup. Table. for reagents and strains details.

Strain construction

Cassettes for expressing GEMs (20 nm, AqLs-Sapphire; 40 nm, PfV-Sapphire; 50 nm, Vuldi-Sapphire), were cloned into the fission yeast pREP41X expression vector from pRS306 budding yeast expression vectors. The Vuldi-sapphire pRS306 plasmid was a kind gift from the Holt lab. Briefly, GEMs expression cassettes were amplified via PCR and inserted into pREP41X via Gibson assembly at the XhoI site. The primers used for PCR are described in the supplementary table.

Protoplast preparation

S. pombe cells were grown in YE5S liquid culture at 30 °C to exponential phase, harvested, and washed with SCS buffer (20 mM citrate buffer, 1 M D-sorbitol, pH 5.8), then resuspended in SCS buffer supplemented with 0.1 g/mL Lallzyme (Lallemand, Montreal, Canada) (Flor-Parra et al., 2014). Cells were digested for 10 min at 37 °C with gentle shaking in the dark. The resulting protoplasts were gently washed twice in YE5S medium with 0.2-1 M D-sorbitol, using gentle centrifugation (2 min at 0.4 rcf).

Imaging of fission yeast

S. pombe cells and protoplasts were imaged in commercial microchannels (Ibidi µ-slide VI 0.4 slides; Ibidi 80606, Ibiditreat #1.5). Channels were pre-treated with 50 µl of 100 µg/ml lectin solution for 5 min at room temperature. The lectin solution was removed by pipetting and 50 µl of cell culture were introduced. After incubation for 3 to 10 minutes to allow cells to adhere to the lectin, the cells were washed with YE5S. For hyper-osmotic shocks, the medium was manually removed from the channel via pipetting and quickly replaced with hyper-osmotic media as indicated.

Microtubule dynamics. Yeast cells expressing GFP-tubulin (see Table) were observed with a 488 nm excitation laser at 100 ms of exposure per z-slice (1 µm spacing, 7 slices) at 0.1 Hz, with a 60x objective (CFI Plan Apochromat VC 60XC WI) on a Nikon TI-E equipped with a spinning-disk confocal head (CSU10, Yokogawa) and an EM-CCD camera (Hammamatsu C9100-13).

Protoplast volume. Protoplasts were resuspended YE5S medium with 0.2-1 M D-sorbitol, then imaged with a 561 nm excitation laser at 100 ms of exposure per z-slice (0.5 µm spacing), with the 60x objective, microscope, and camera used for MT dynamics.

GEMs diffusion. Yeast cells were imaged with a 60x TIRF objective (Nikon, MRD01691) on a Nikon TI-E equipped with a Nikon TIRF system and a SCMOS camera (Andor, Ixon Ultra 888). Protoplasts were imaged on a Nikon TI-2 equipped with a Diskovery Multi-modal imaging system from Andor and a SCMOS camera (Andor, Ixon Ultra 888) using a 60x TIRF objective (Nikon, MRD01691). Cells were imaged at 100 Hz, in TIRF, for 10 s with a 488 nm excitation laser.

Tubulin diffusion. Cells were imaged at 0.2 Hz, with a 60x TIRF objective (Nikon, MRD01691) on a Nikon TI-2 equipped with a Diskovery Multi-modal imaging system from Andor and a SCMOS camera (Andor, Ixon Ultra 888). Cells were imaged using spinning disk with pinhole of 100 μm. Cells were imaged at 488 nm laser excitation; the bleaching laser was a 473 nm laser controlled by a UGA-42 Firefly (Rapp OptoElectronic).

Osmotic shock experiments

Hyperosmotic shifts. Cells were grown in rich YE5S medium, mounted into microchannels, and then treated with YE5S containing various concentrations of sorbitol while on the microscope stage at room temperature. Loss of water after the switch of medium is almost instantaneous (<30 s). To minimize adaptation responses (Tatebe et al., 2005), imaging was initiated as soon as possible (<1 min) after adding sorbitol.

Osmotic oscillations. Cells were introduced into a microfluidic system (Cell Asics) as described in (Knapp et al., 2019) then the media in the chamber was oscillated; YE for 5 minutes then YE with 1.5 M sorbitol for 3 minutes. During the oscillations cells were imaged for MT dynamic measurement as described in above.

Cold treatment. Yeast cells expressing GFP-tubulin were pelleted gently and resuspended in YE containing 0, 0.5, 1, or 1.5 M sorbitol. Each culture was split into two tubes; one was incubated for 5 min at room temperature and the other was incubated on ice for 5 min. Cells were fixed by adding 16% paraformaldehyde to the medium for a final concentration of 4%. Cell were then imaged in lectin-treated Ibidi chambers.

Osmotic shifts of protoplasts. After cell-wall digestion, protoplasts were gently washed twice in YE5S with 0.4 M D-sorbitol using gentle centrifugation (2 min at 0.4 rcf), then placed in the Ibidi chamber for imaging. Medium was exchanged manually with hypo- or hyper-tonic medium right before imaging. YE + 0.4 M sorbitol was close to isotonic conditions, as determined by comparing volumes and GEMs dynamics to yeast cells. Thus, protoplasts resuspended in YE + 0.2, 0.25, or 0.3 M sorbitol were in hypo-tonic conditions, while protoplasts in YE + 0.5 or 1 M sorbitol were in hyper-tonic conditions.

Measurements of MT dynamic parameters and cell volume in yeast and protoplasts

MT dynamics. Measurements of MT dynamic parameters were obtained using analyses of kymographs of GFP-tubulin expressing cells. Images of individual cells were cropped and multiple MT bundles per cell were selected. Kymographs were made and analyzed with the KymoToolBox plugin of ImageJ (Schneider et al., 2012).

Volume. The effects of sorbitol on cell volume were determined from brightfield images (Atilgan et al., 2015). Protoplast volume was measured in 3D from Z-stack fluorescence images of cells expressing markers for the plasma membrane (mCherry-Psy1) using LimeSeg, a Fiji pulg-in (Schindelin et al., 2012) (Machado et al., 2019).

FLIP experiments

Cells expressing GFP-tubulin were mounted in microchannels and treated with 25 μg/ml methyl benzimidazol-2-yl-carbamate (MBC) for >1 min to depolymerize MTs. Cells were then subjected to repeated photobleaching with a focused 473 nm laser in a 1-μm region near the cell tip using a UGA-42 Firefly system from RapOpto. Cells of similar size (~ 12 μm long) were photobleached in order to reduce variability in the resulting data. Fluorescence decay was followed in the half of the cell submitted to the

bleaching sequence to avoid the effects of diffusion around/through the nucleus. Fluorescence decay curves were normalized and aligned to the time point preceding the activation of the bleach sequence.

A calibrated 1D Brownian model of diffusion was used to simulate the fluorescence decay in a 6 μm tube (half of a cell 12 m in length). Bleaching rate, region size, and position were matched to the experimental setup. Particles positions were updated every 0.01 s. The decay in the number of unbleached particles in the model was read out every 5 s (matching the imaging frequency) and normalized to the total number of particles. The insensitivity of the model to the total number of particles and to the time interval used was established by changing these parameters across three orders of magnitude, without significant effect on the outputs. Decay plots for various diffusion rates in the model were compared to the experimentally measured values to obtain the estimated tubulin diffusion rates.

Microrheology with GEMs nanoparticles.

GEM fusion proteins were expressed from pREP41X-based expression vectors from the thiamine-regulated nmt1* promoter (Maundrell, 1990). Transformants containing these plasmids were maintained on EMM-leu medium. The day before imaging, cells were inoculated in EMM-leu medium containing 0.05 μg/mL thiamine to allow a low level of construct expression. These conditions generally produced a few tens of GEM nanoparticles per cell. Overexpression of the GEMs commonly produced cells with single, bright, non-motile aggregates. Cells expressing GEMs were selected for sparse numbers of labeled motile nanoparticles and imaged at 100 Hz intervals. Individual cells were cropped for analysis. Nanoparticles in each cell were tracked using the MOSAIC plugin (Fiji ImageJ), and the effective diffusion rate was determined from mean squared displacement (MSD) plots as previously (Delarue et al., 2018). Briefly, tracks shorter than 10 timepoints were excluded from the MSD analysis. The following fit was used on the first 100 ms to extract the diffusion value for trajectories longer than 10 timepoints: MSD = 4Dt. The following parameters were used for the 2D Brownian dynamics tracking in MOSAIC: radius = 3, cutoff = 0, per/abs = 0.2-0.3, link = 1, and displacement = 6.

MT dynamics in moss cells

Moss cells were grown as described previously (Yamada et al., 2016). Caulonemal cells were mounted in microfluidic devices at room temperature as described previously (Kozgunova and Goshima, 2019). For osmotic shock, observation medium was removed manually via aspiration with a syringe, and medium with sorbitol was subsequently introduced with a syringe. Cells were imaged on a Nikon TI-E TIRF system with a 60x TIRF objective (Nikon, MRD01691) and a SCMOS camera (Andor, Ixon Ultra 888).

MT dynamics *in vitro*

Tubulin preparation. Tubulin was purified from juvenile bovine brains via cycles of polymerization and depolymerization, as described previously (Ashford and Hyman, 2006). GMPCPP-stabilized MT seeds were prepared by polymerizing a 1:4 molar ratio of tetramethylrhodamine (TAMRA, ThermoFisher Scientific) labeled:unlabeled tubulin (Hyman, 1991) in the presence of GMPCPP (Jena Biosciences) in two cycles, as described previously (Gell et al., 2011).

MT reconstitution assay. Dynamic MTs were imaged in a reconstitution assay from surface-bound, stabilized MT seeds (Gell et al., 2011). Cover glass was cleaned, as previously described (Helenius et al., 2006). Two silanized cover glasses (22 x 22 mm and 18 x 18 mm) were separated by multiple strips of double-sided tape on custom-machined mounts to create channels for solution exchange. Channels were prepared for experiments by flowing in anti-TAMRA antibodies (ThermoFisher Scientific) and blocking with 1% Pluronic F-127 for 20 min. Channels were rinsed three times with BRB80 before flowing in seeds

and placing the chamber on the microscope stage, where the objective was heated to 32 °C with a CU-501 Chamlide lens warmer (Live Cell Instrument).

Dynamic MTs were grown from GMPCPP seeds by filling the channel with 10 μM tubulin in reaction buffer: BRB80 (80 mM PIPES-KOH [pH 6.9], 1 mM EGTA, 1 mM $MgCl_2$) plus 1 mM GTP, 0.1 mg/mL bovine serum albumin, 10 mM dithiothreitol, 250 nM glucose oxidase, 64 nM catalase, and 40 mM D-glucose. Reaction buffer was prepared on ice before being flowed into the channel with a piece of filter paper. A 60% (v/v) glycerol stock solution in BRB80 was added to the indicated final concentrations. For consistency, a large aliquot of tubulin was thawed on the day of each experiment, sub-aliquoted, and stored in liquid nitrogen. A separate sub-aliquot was thawed for each individual experiment. Glycerol concentrations from 0-15% (v/v) were tested. We note that the effects of glycerol concentrations ≥20% were not measurable as no shrinkage events were observed because of the high levels of spontaneous nucleation and inhibition of catastrophes at those glycerol concentrations.

Interference reflection microscopy. Dynamic label-free MTs were imaged with interference reflection microscopy (IRM) as described previously (Mahamdeh and Howard, 2019).

MT dynamics. MT dynamics was analyzed using kymographs as described above.

Tubulin diffusion. Tubulin diffusion rate *in vitro* was estimated using the Stoke-Einstein equation $D = {K_B T}/{6\pi\eta r}$, where T is the experimental temperature (32 °C), η is the viscosity of the buffer, and r is the radius of a sphere equivalent to the volume of a tubulin dimer (3 nm). Pairwise correlations among MT polymerization rate, depolymerization rate, and tubulin diffusion were analyzed using Pearson's test performed with GraphPad Prism.

Cytoplasm viscosity measurements

Wild-type fission yeast cells were grown in YE overnight at room temperature with agitation to below saturation.

FDA labeling. Cells were labeled with 100 μM fluorescein diacetate (Sigma, F7378) for 30 min at room temp with agitation.

Time-resolved fluorescence anisotropy. Cells were imaged in a Ibidi μ-slide VI 0.4 (Ibidi 80606, Ibiditreat #1.5) treated with lectin on an inverted TCS-SP2 microscope (Leica Microsystems, Germany) while the time- and polarization-resolved intensity decay was measured on SPC-150 TCSPC boards (Becker & Hickl, Germany). The emission was split using a polarizing beam splitter. Fluorescein diacetate (FDA) was excited using a picosecond-pulsed (90 ps optical pulse width, 20 MHz repetition rate) 467 nm diode laser (Hamamatsu, Japan) through a 63X 1.2 NA water objective, with a 485 nm dichroic mirror and a 500 nm long pass filter. All measurements were performed at room temperature.

Parallel ($I_\parallel$) and perpendicular ($I_\perp$) intensity decays were used to calculate the anisotropy decay, according to

$$r(t) = (I(t)_\parallel - G * I(t)_\perp)/(I(t)_\parallel + z * G * I(t)_\perp)$$

where z = 1 to account for the depolarization of the high magnitude objective and G was 0.96. Z was determined by comparing the calculated total intensity decay

$$I_{tot} = I_\parallel + z * GI_\perp$$

of fluorescein measured on the 63x objective and measured on a 5x objective, altering the value of z between 2 and 1 until the lifetime was an exact match (Suhling et al., 2014). G is a correction factor to account for the sensitivity of the two detectors and is calculated by taking the tail value of

$$G = I(t)_{\parallel}/I(t)_{\perp}$$

after tail-matching of the parallel and perpendicular decays by adjustment of the polarizing beam splitter.

The resulting time-resolved anisotropy decay was fit to a monoexponentially decaying model according to

$$y = A * exp^{\left(-\frac{t}{\theta}\right)} + y_0$$

where θ is the rotational correlation time, A is the amplitude of the decay (in terms of the anisotropy decay, this value is equal to r_0-r□), and y_0 is the level to which the anisotropy decays (properly known as r). The rotational correlation time was converted into a viscosity value in cP using a calibration plot in the relevant viscosity region.

Fluorescein calibration curve. Methanol solutions containing various amounts of glycerol (0-30%) were prepared. Solution viscosities at room temperature (22 °C) were established previously using a rheometric expansion system rheometer (ARES) (Kuimova et al., 2008) (Steinmark et al., 2020). Fluorescein (10 μM) was added to the solutions and fluorescence was measured at room temperature to extract the rotational correlation times as described above. Note that the calibration was carried out on a 5x air objective; thus, z was taken as 2.

Anisotropy decay. Anisotropy data were fitted using GraphPad Prism. Fits used $1/STD^2$ weighting and were limited to the first 10 ns of recording. Best-fit values for each parameter and condition were compared via two-way ANOVA with Sidak's multiple comparison test. Decay rate were different with p-value < 0.0001.

Acknowledgments

We thank members of the Chang and Dumont labs for fruitful discussions. We are grateful to Dr. Rikki Garner for countless discussions and her help setting up the stochastic model of diffusion, and to Dr, Fabrice Cordelières for the KymoToolBox ImageJ plug-in. We thank Sherman Foo and the Oliferenko lab for reagents and technical support. We are grateful to Steve Ross and Nikon who generously lent us a microscope at MBL. We are thankful MBL communities from the Physical Biology of the Cell Course, from the Physiology Course and from the Whitman Investigator Program for support and advice.

Competing Interests

The authors declare no financial or competing interests.

Author Contributions

Conceptualization: A.T.M. and F.C.; Methodology: A.T.M., J.L, C.E., C-T.H., I.E.S., K.S., G.G., L.H., G.J.B., and F.C.; Formal analysis: A.T.M., J.L, I.E.S; Investigations: A.T.M., C.E., I.E.S; Writing: A.T.M., G.J.B., and F.C.; Review editing: A.T.M., C.E., G.J.B., and F.C.; Visualization: A.T.M.; Supervision: A.T.M.; Project administration and funding acquisition: F.C.

Funding

This work was supported by a grant to F.C (NIH R01GM115185) and to L.J.H. (R01 GM132447 and R37 CA240765).

Supplemental Information

Refers to the webpage for description and access to the supplemental material.

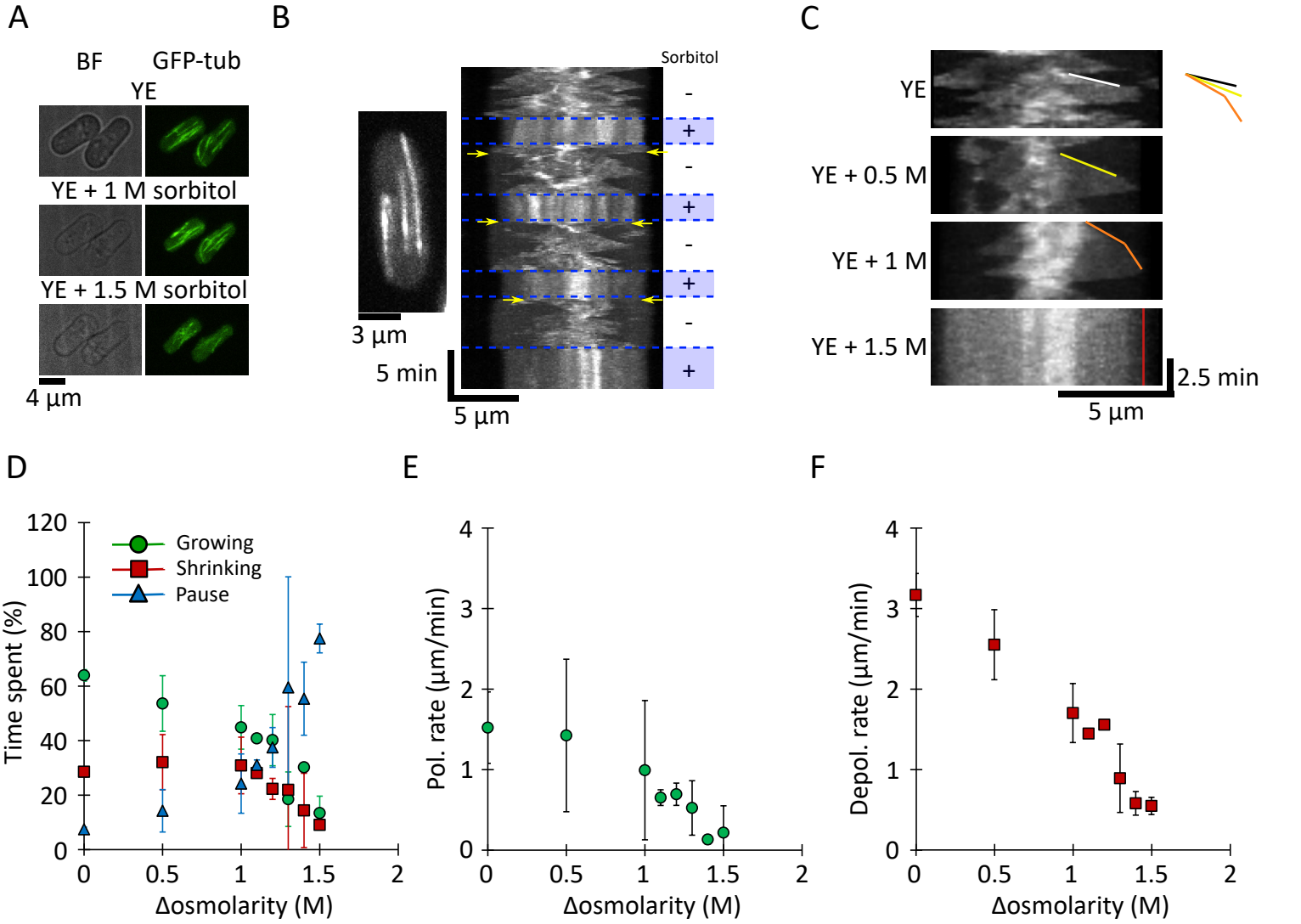

Figure 1: MT growth and shrinkage rates decrease upon hyperosmotic shock in yeast cells.
(A) Brightfield (BF; left) and fluorescence (right) images of interphase MT bundles in two fission yeast cells expressing GFP-tubulin (GFP-tub) upon sequential treatment with YE (medium alone), YE + 1 M sorbitol, and YE + 1.5 M sorbitol.
(B) MT dynamics in a cell treated with oscillations of YE (5 min) and YE + 1.5 M sorbitol (3 min). In the kymograph, this representative cell is expressing GFP-tubulin; the cell image has been collapsed onto a line. MTs exhibit decreased dynamics acutely in 1.5 M sorbitol. Upon sorbitol washout, MTs first depolymerize (yellow arrows) and then resume dynamic behaviors.
(C) Kymographs of MTs in cells at the indicated sorbitol concentrations. Lines highlight tracks of single growing MT plus-ends. Colored lines highlight growth events.
D) Percentage of time that interphase MTs spent growing (green circles), shrinking (red squares), or paused (blue triangles) in YE and after hyperosmotic shocks (AVG +/- standard deviation). Cell and MT values of n are as in (E).
(E) MT polymerization rates (green circles) in cells treated acutely with the indicated sorbitol concentrations. Values are AVG +/- standard deviation. Data come from (left to right) n = 58 / 51 / 32 / 27 / 38 / 23 / 15 / 26 cells and 118 / 99 / 60 / 65 / 72 / 34 / 22 / 44 MT, respectively, from at least 2 experiments.
(F) MT depolymerization (red squares) rates in cells treated acutely with the indicated sorbitol concentrations. Values are AVG +/- standard deviation. Cell and MT values of n are as in (E).

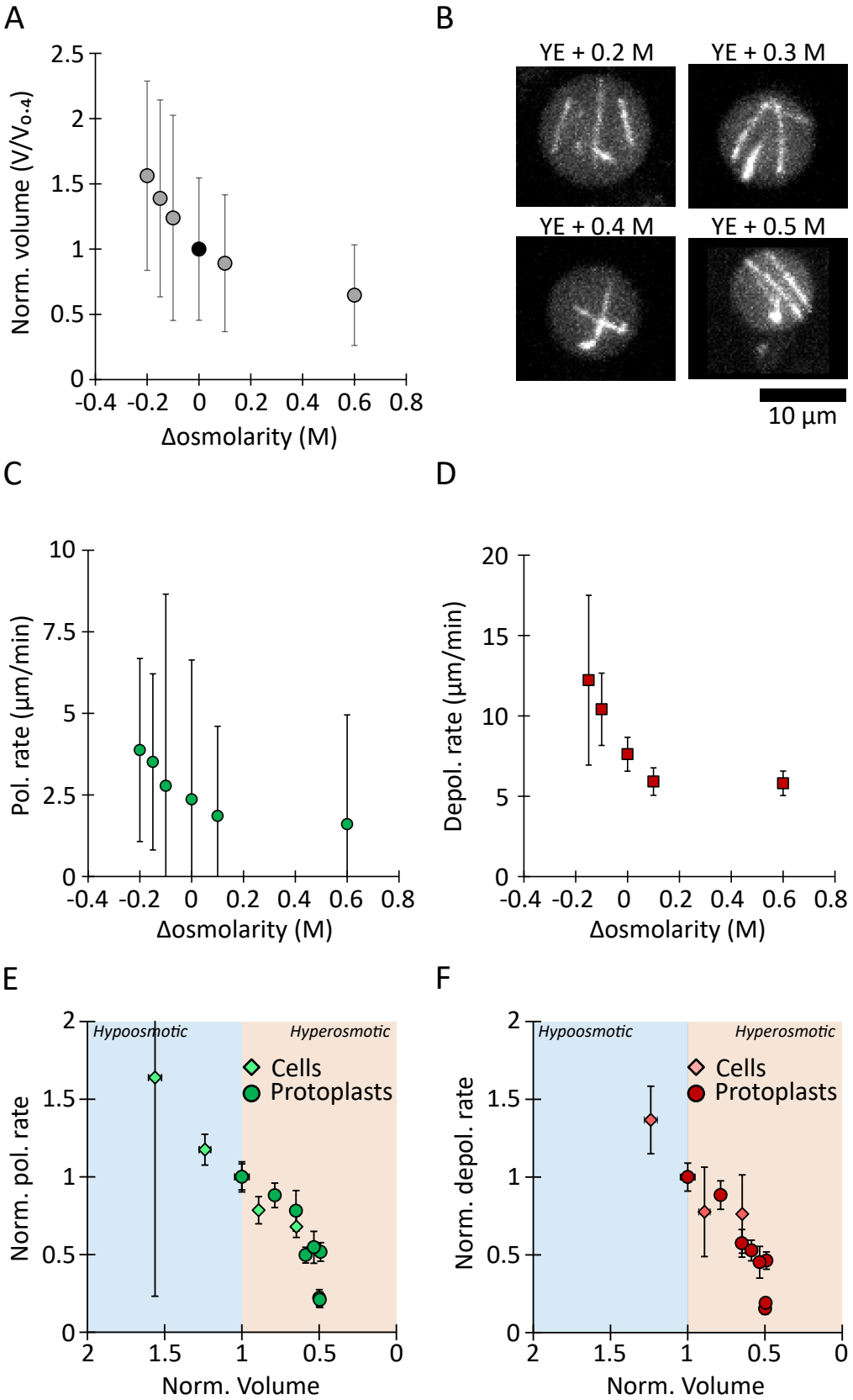

Figure 2: MT growth and shrinkage rates scale with cell volume in yeast protoplasts.
(A) Normalized protoplast volume. Data were normalized to osmolarity conditions of 0.4 M sorbitol, in which the average volume distribution of protoplasts matched that of intact cells (AVG +/- standard deviation). Data come from at least two experiments; (left to right) n = 18 / 45 / 109 / 446 / 200 / 440 protoplasts.
(B) Representative images of GFP-labelled MTs in protoplasts in medium supplemented with the indicated sorbitol concentrations.
(C) MT polymerization (Pol.) and (D) depolymerization (Depol.) rates in yeasts protoplasts in medium supplemented with the indicated sorbitol concentrations. Values are AVG +/- standard deviation. Left to right, n = 10 / 13 / 64 / 29 / 28 / 25 polymerization events and n = 7 / 57 / 25 / 13 / 12 depolymerization events from three experiments.
(E) MT polymerization rate and (F) depolymerization rates, normalized to the isotonic condition for yeast cells (circles) and yeast protoplasts (diamonds), as a function of the normalized volume. Both rates are increase in hypo-tonic conditions (blue shading) and decrease in hyper-tonic conditions (orange shading).

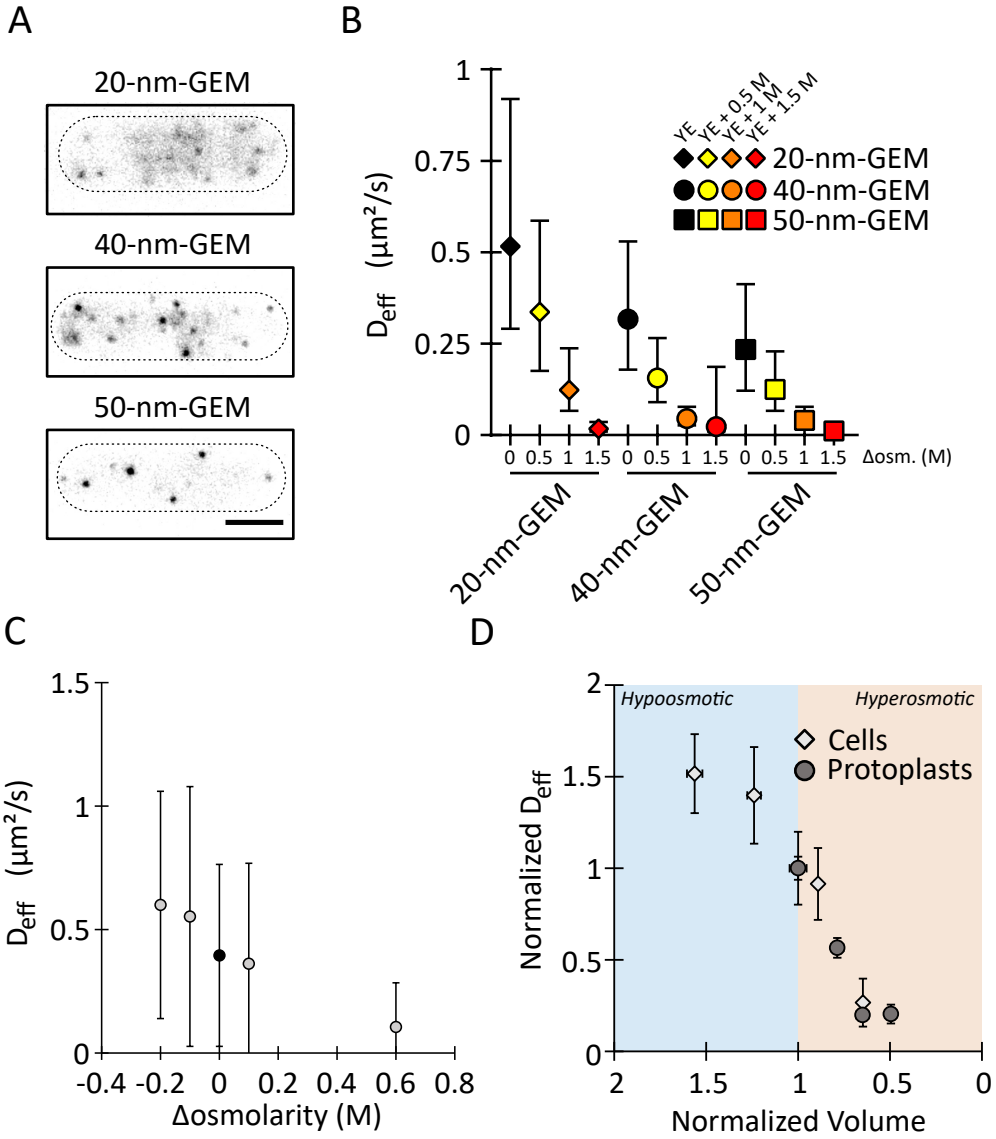

Figure 3: Nanoparticles diffusion rate scales with cytoplasm concentration.
(A) Representative images of GEMs in fission yeast cells. Scale bar, 5 µm.
(B) Hyperosmotic shifts decrease the effective diffusion coefficients of GEMs of indicated sizes in yeast cells. Values are AVG +/- standard deviation. Data come from three experiments, n > 1000 trajectories, and n > 49 cells. Concentrations reflect sorbitol concentrations in the medium.
(C) Effective diffusion coefficients of 40-nm GEMs in yeast protoplasts as a function of sorbitol. AVG +/- standard deviation. Data come from at least two experiments and (left to right) n = 643 / 411 / 304 / 488 / 162 trajectories.
(H) Diffusion rate of the 40-nm GEMs in yeast cells (circles) and yeast protoplasts (diamonds) normalized to the iso-tonic condition as a function of the normalized volume. The rate of diffusion through the cytoplasm is faster in hypo-tonic conditions (blue shading) and slower in hyper-tonic conditions (orange shading).

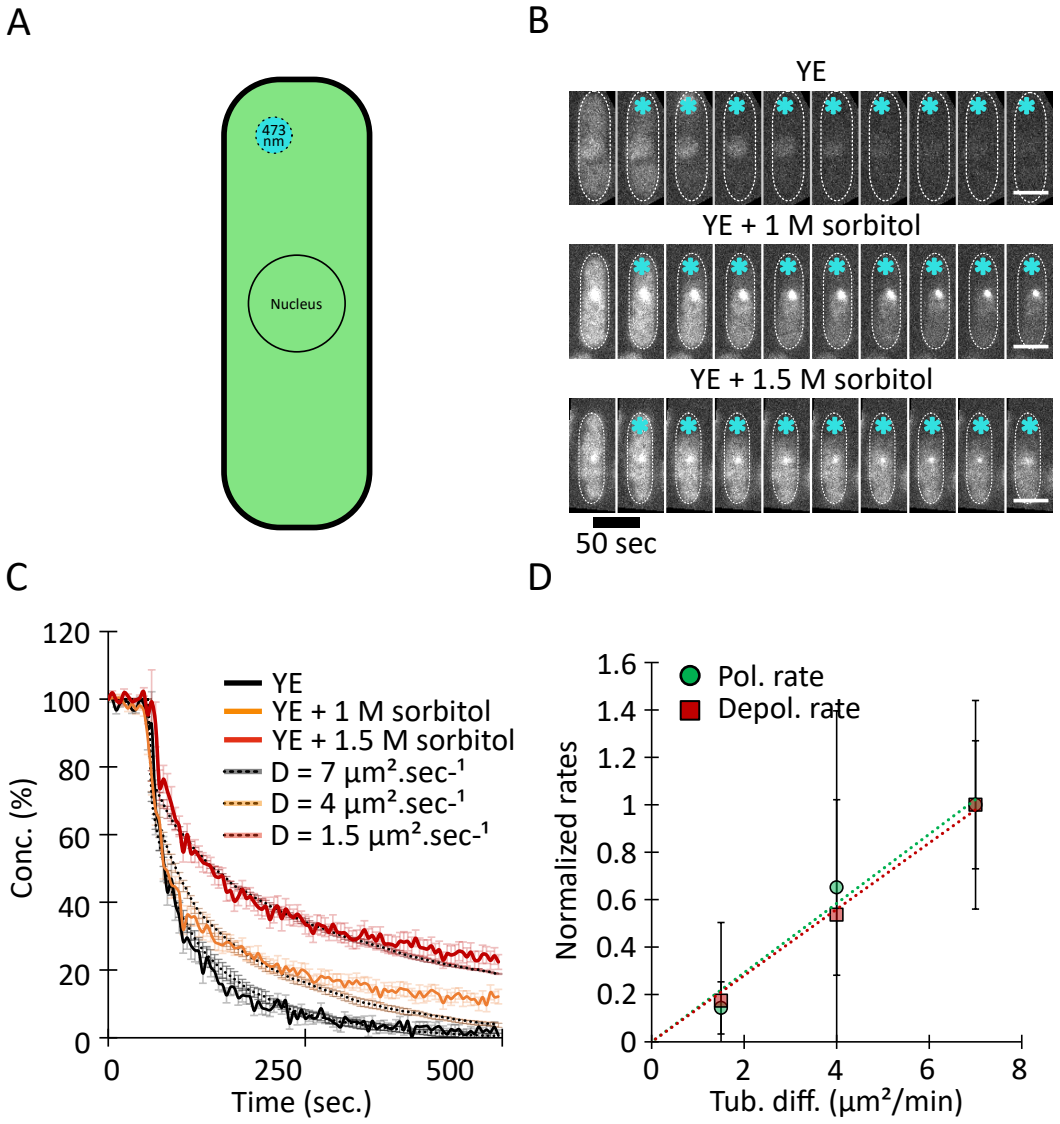

Figure 4: Hyperosmotic shifts decrease the diffusion rate of soluble tubulin.
(A) To measure the diffusion of soluble GFP-tubulin, we used FLIP. Cells were exposed repeatedly to a focused laser beam (~1 µm) near one cell tip and GFP fluorescence intensity was measured (Methods).
(B) Fluorescence decay of cells expressing GFP-tubulin in a representative FLIP experiment at the indicated sorbitol conditions. Interphase cells in which MTs were depolymerized with 25 µg/ml methyl benzimidazol-2-yl-carbamate (MBC) were photobleached using a focused laser (blue stars). Scale bars, 4 m.
(C) Loss of fluorescence intensity in cells from three osmotic conditions and the corresponding tubulin diffusion rate. Values (AVG +/- standard deviation) were normalized to initial intensity and expressed as concentrations (%). Data are n = 46 / 29 / 29 cells, for YE alone, YE + 1 M sorbitol, and YE + 1.5 M sorbitol, respectively, from three independent experiments. Dashed lines denote predictions from simulations of a 1D model (Methods) for various values of diffusion; these predictions were used to estimated diffusion rates from our experimental data. Simulation values are AVG +/- standard deviation for 5 simulations.
(D) Rates of MT polymerization and depolymerization in yeast cells as a function of tubulin diffusion rate. Data come from Figures 1 and 4. Correlations between diffusion and polymerization rate (P = 0.008) and depolymerization rate (P = 0.001) are significant according to Pearson's correlation test.

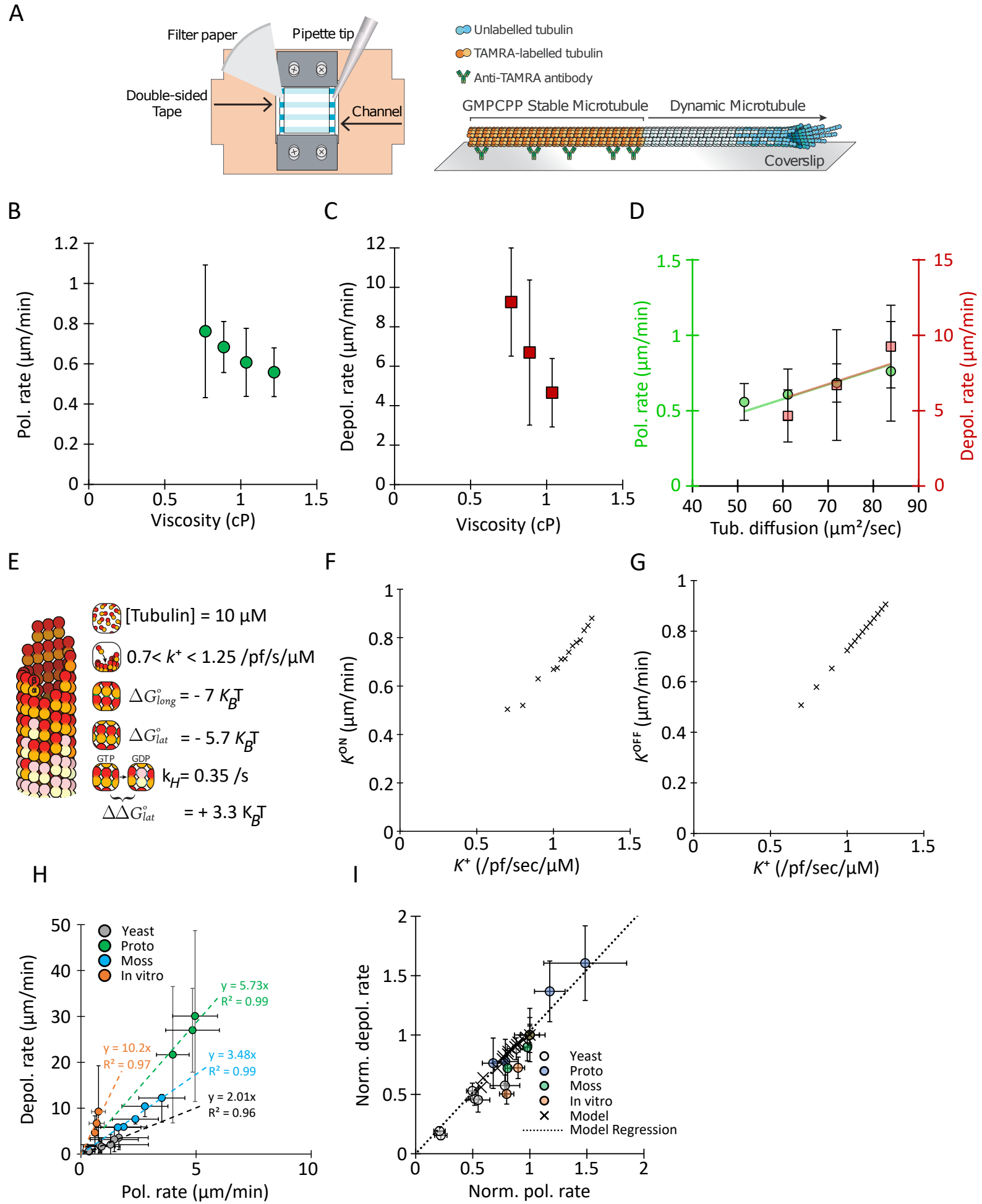
A
Filter paper
Pipette tip
Double-sided Tape
Channel
Unlabelled tubulin
TAMRA-labelled tubulin
Anti-TAMRA antibody
GMPCPP Stable Microtubule
Dynamic Microtubule
Coverslip
B
Pol. rate (µm/min)
Viscosity (cP)
C
Depol. rate (µm/min)
Viscosity (cP)
D
Pol. rate (µm/min)
Depol. rate (µm/min)
Tub. diffusion (µm²/sec)
E
[Tubulin] = 10 µM
0.7< k⁺ < 1.25 /pf/s/µM
ΔG°long = - 7 KBT
ΔG°lat = - 5.7 KBT
GTP
GDP
kH= 0.35 /s
ΔΔG°lat = + 3.3 KBT
F
KON (µm/min)
K⁺ (/pf/sec/µM)
G
KOFF (µm/min)
K⁺ (/pf/sec/µM)
H
Yeast
Proto
Moss
In vitro
y = 5.73x
R² = 0.99
y = 10.2x
R² = 0.97
y = 3.48x
R² = 0.99
y = 2.01x
R² = 0.96
Depol. rate (µm/min)
Pol. rate (µm/min)
I
Yeast
Proto
Moss
In vitro
Model
Model Regression
Norm. depol. rate
Norm. pol. rate

Figure 5: Increasing viscosity dampens rates of MT polymerization and depolymerization.
(A) Schematic of the in vitro reconstituted system for MT dynamics measurement.
(B) MT polymerization rates (green circles) and (C) MT depolymerization rates (red squares) were measured in MTs in solutions of varying viscosity. Data represent 3 repetitions with n > 70 MTs per condition
(D) Rates of microtubule polymerization and depolymerization in vitro as a function of tubulin diffusion rate. Correlation is significant, p-value = 0.002 and 0.02 for polymerization and depolymerization rates respectively (Pearson correlation test).
(E) Schematic of the parameters used to model MT dynamic instability. Changing the association rate constant k+ was used to model the effect of viscosity. For more details see Methods.
(F) Apparent on-rate as a function of the association rate constant in the model.
(G) Apparent off-rate as a function of the association rate constant in the model.
(H) Scatter plot of the observed depolymerization rates versus the observed polymerization rates for the experiments in this study (moss (green circles), yeast cells (grey circles), yeast protoplasts (blue circles), in vitro (orange circles)). Each model presents a certain ratio (the slope of the regression) of depolymerization rate to polymerization rate but this ratio (the slope of the regression) is conserved when viscosity is increased in vitro or when cell volume is reduced by hyper-osmotic shocks (yeast, protoplasts, and moss). AVG +/- STD.
(I) Cytoplasm and viscosity have similar effects of MT polymerization and depolarization rates. Graph shows the relationship between normalized depolymerization rates and normalized polymerization rates for all the experimental conditions and the model prediction. AVG +/- propagated error.